https://doi.org/10.5194/egusphere-2025-608
Preprint. Discussion started: 25 March 2025

Numerical simulation of nitrous oxide over Asia using regional climate-chemistry-ecology coupling model RegCM-Chem-YIBs

Xin Zeng[1], Tijian Wang[1*], Congwu Huang[2], Bingliang Zhuang[1], Shu Li[1], Mengmeng Li[1], Min Xie[3], Qian Zhang[1], Nanhong Xie[1]

[1]School of Atmospheric Sciences, Nanjing University, Nanjing, China.

[2] Hubei Key Laboratory of Regional Development and Environmental Response, Faculty of Resources and Environmental Science, Hubei University, Wuhan 430062, China.

[3] School of Environment, Nanjing Normal University, Nanjing, China

Corresponding to: Tijian Wang (tjwang@nju.edu.cn)

Abstract. Nitrous oxide (N_2O) is a significant greenhouse gas that not only contributes to global warming but also depletes the ozone layer. In our study, we enhanced a regional climate-chemistry-ecology model to better understand how N_2O is emitted, transported, and dispersed in the atmosphere. We focused on East Asia, South Asia, and Southeast Asia, using two different datasets to analyze the patterns of N_2O in 2020. Our model showed good agreement with real-world observations, revealing that N_2O levels vary seasonally and spatially. For example, the lowest concentrations were found in June, while the highest were in December. Certain areas, like the North China Plain and the Ganges River Basin, had higher N_2O levels. We also found that N_2O concentrations decrease with altitude. By validating our model, we gained insights into the complex interactions between N_2O emissions and atmospheric processes. This research helps policymakers develop strategies to reduce N_2O emissions. In the future, we aim to refine our model further to improve predictions of N_2O emissions and distribution, which will support efforts to combat climate change and protect the ozone layer.1 Introduction

Nitrous oxide (N_2O) ranks as the third most prevalent greenhouse gas in the atmosphere, following carbon dioxide (CO_2) and methane (CH_4). It possesses a warming potential 273 times greater than that of carbon dioxide and contributes approximately 6% to the radiative forcing of long-lived greenhouse gases (WMO, 2023; NOAA, 2024), with an atmospheric lifetime of 116±9 years (Prather et al., 2015). By 2022, the global average concentration of N_2O had reached 335.8±0.1 parts per billion (ppb), reflecting a 124% increase since the 1850s. This makes N_2O the primary driver of the increase in the

https://doi.org/10.5194/egusphere-2025-608
Preprint. Discussion started: 25 March 2025

effective radiative forcing of long-lived gases since 1990 (Wmo, 2023). In addition to its role as a potent greenhouse gas, N_2O is also a significant ozone-depleting substance. Its photolysis in the stratosphere generates NO_x, which contributes to ozone depletion (Mcelroy and Mcconnell, 1971; Unep, 2013). In 2020, anthropogenic N_2O emissions, expressed in terms of CFC-11 equivalents, exceeded those of all CFCs by more than twofold, representing over 20% of the peak CFC emissions recorded in 1987 (Geneva, 2022). Currently, N_2O emissions are the most substantial among ozone-depleting substances (ODS_s) and are anticipated to remain the largest throughout the 21st century (Ravishankara et al., 2009). The escalating concentration of N_2O exerts a profound impact on global warming, air pollution, and ozone layer depletion, prompting extensive global concern. In response, the international community has implemented various conventions and agreements to regulate N_2O emissions, aiming to mitigate its detrimental effects on the climate and ozone layer. The United Nations Framework Convention on Climate Change (UNFCCC), along with its Kyoto Protocol and the Paris Agreement (Idowu et al., 2023), constitute three pivotal international legal instruments in the fight against climate change. These frameworks guide global efforts to reduce emissions. The UNFCCC is dedicated to controlling greenhouse gas emissions to combat global warming, the Kyoto Protocol establishes specific reduction targets for developed countries, including N_2O, and the Paris Agreement reinforces the global commitment to emission reduction by requiring nations to formulate and execute their Intended Nationally Determined Contributions (NDCs) to cap the increase in global average temperature.

As a greenhouse gas of significant global concern, accurately simulating the emission and concentration distribution of N_2O is essential for assessing the impacts of climate change and crafting effective emission reduction strategies (De Sisto et al., 2024; Zhou et al., 2020). Tian (2020) quantified global natural and anthropogenic sources and sinks of N_2O from 1980 to 2016, using both top-down and bottom-up approaches. Their findings indicate that global anthropogenic emissions, primarily driven by nitrogen inputs from agricultural activities, have increased by 30% during this period, leading to a growing atmospheric burden. The imbalance between N_2O sources and sinks has contributed to the rise in its atmospheric concentration. Previous research has predominantly concentrated on modeling N_2O emissions to diminish uncertainty. This includes relatively simple empirical models such as the DAISY model (Hansen et al., 1991) and the CRISP model (Nielsen et al., 1999), as well as process-based models like DAYCENT (Parton et al., 1996), DNDC (Stange et al., 2000), ECOSYS (Grant et al., 2001), MiCNiT

https://doi.org/10.5194/egusphere-2025-608
Preprint. Discussion started: 25 March 2025

(Blagodatsky et al., 2011), and the Dynamic Land Ecosystem Model (DLEM) (Tian et al., 2013). While the simulation of N_2O emissions has seen consistent improvement, there remains a scarcity of models capable of accurately simulating N_2O concentrations. Therefore, the development of high-resolution atmospheric chemical models is crucial for simulating the concentration distribution of N_2O in the atmosphere. Precise simulation of N_2O emissions and concentration dynamics is vital for forecasting its potential environmental impacts and providing a scientific foundation upon which to base the development of effective environmental policies.

Research (Tian et al., 2020; Weber et al., 2024) indicates that East Asia (EA) and South Asia (SA) are the primary contributors to global N_2O emissions. Agricultural activities in these regions, particularly the application of fertilizers and the use of livestock manure, are highly concentrated, which are the predominant sources of N_2O (De Sisto et al., 2024; Zhang et al., 2022). In China and India, emissions from fertilizer use are dominant, with agriculture accounting for approximately 70% of anthropogenic N_2O emissions (Tian et al., 2020). Consequently, agricultural practices in these areas have a substantial impact on the global N_2O emission profile. EA is responsible for 71-79% of global aquaculture N_2O emissions, while SA and Southeast Asia (SEA) together contribute 10-20% (Beusen et al., 2016; Macleod, 2019). The densely populated and rapidly developing economies of EA, SA and SEA have led to an increased demand for food and animal feed, further intensifying agricultural activities and the associated N_2O emissions (Tian et al., 2020). As both a significant greenhouse gas and a stratospheric ozone-depleting substance, N_2O presents additional challenges to environmental sustainability and regional climate in EA (Bi et al., 2013). Therefore, monitoring and modeling the concentration distribution of N_2O is essential for comprehending and predicting climate change trends (Ma et al., 2021). Satellite data inversion reveals that N_2O concentrations exhibit significant temporal and spatial variability, influenced not only by local emissions but also by regional transport from external areas. This underscores the importance of regional and global cooperation in mitigating N_2O emissions and safeguarding the ozone layer. Consequently, simulating and studying N_2O concentration patterns in EA, SA and SEA will not only assist in pinpointing key emissions and transport pathways but also provide a scientific foundation for developing effective regional climate policies and measures to protect the ozone layer (Weber et al., 2024).

In this study, we employ an advanced coupled regional climate-chemical-ecosystem model,

https://doi.org/10.5194/egusphere-2025-608
Preprint. Discussion started: 25 March 2025

RegCM-Chem-YIBs, to simulate and analyze N_2O concentrations in EA, SA and SEA during 2020. The primary objective is to evaluate the atmospheric response to the rapid increase in terrestrial N_2O emissions. Our research is designed to accurately simulate the fluctuations in N_2O concentrations, thereby enabling the prediction of their potential environmental impacts and laying a scientific groundwork for the development of impactful environmental policies. Furthermore, the findings of this study are poised to offer invaluable insights for the formulation of greenhouse gas (GHG) reduction strategies. The methodologies and datasets utilized in this research are meticulously outlined in Section 2, while the ensuing results are thoroughly examined in Section 3. Concluding remarks, summarizing our key findings and their implications, are presented in Section 4.

2 Model and Methods

2.1 Model description

This study employs the regional climate-chemistry-ecology coupling model (RegCM-Chem-YIBs) (Xie et al., 2019) which analyze the temporal and spatial distribution of short-lived air pollutants and their interactions with the long-lived greenhouse gas CO_2. Additionally, it investigates the processes and mechanisms underlying the interactions between air pollutants, greenhouse gases, and regional climate. To enhance air pollution control and respond to climate change more effectively, the regional climate chemical model RegCM-Chem (Shalaby et al., 2012) is integrated with the ecological model YIBs (Yue and Unger, 2015), resulting in the development of a regional climate-chemical-ecological coupling framework. Employing this advanced model, the authors have unveiled the spatial and temporal distribution characteristics and influencing factors of terrestrial CO_2 concentration and terrestrial carbon flux in China over recent years (Xie et al., 2019; Xie et al., 2020). They have also quantitatively analyzed the interaction effects of O_3, $PM_{2.5}$, and CO_2 on the East Asian summer monsoon climate (Ma et al., 2023b; Ma et al., 2023a). Drawing on the representative concentration pathway climate scenario RCP4.5, the study simulates and forecasts the impacts of future regional emission reduction policies and global climate change on air pollution and climate change in China, aligning with the "dual-carbon" goal (Xu et al., 2022; Xu et al., 2023). Furthermore, the model was utilized to explore the interaction dynamics of CO2, ozone, and particulate matter through terrestrial

https://doi.org/10.5194/egusphere-2025-608
Preprint. Discussion started: 25 March 2025

vegetation (Xie et al., 2024). The incorporation of heterogeneous methane (CH_4) allows for a comprehensive assessment of the radiative and chemical impacts of CH_4 on terrestrial carbon fluxes across East Asia (EA), South Asia (SA), and Southeast Asia (SEA) in 2010 (Zhang et al., 2024).

N_2O in the atmosphere is governed by a complex interplay of factors, such as sources, sinks, transport processes, and chemical reactions, leading to a non-uniform spatiotemporal distribution. In this study, we introduce a new species of N_2O into the coupled RegCM-Chem-YIBs model, taking into account the emissions, atmospheric transport, and diffusion processes of N_2O. The enhanced model was employed to simulate N_2O over a one-year period, and a comprehensive analysis of its spatial and temporal distribution in the atmosphere was conducted.

2.2 Experimental design

The model utilized in this study features a horizontal resolution of 36 kilometers, with the upper boundary of the model domain set at 50 hPa. It is composed of a total of 18 vertical layers, centered on the grid point (31° N, 101° E). Employing the Lambert projection, the model simulates the entire region of EA, as well as the majority of SEA and SA. The simulation period spans one year, from January 2020 to December 2020, capturing the spatial and temporal distribution of N_2O within the study area for that year. For this experiment, the model integrates several advanced schemes and modules: the CBM-Z vapor phase chemistry scheme (Zaveri and Peters, 1999) for chemical processes, the Holtslag PBL boundary layer scheme (Holtslag et al., 1990) for boundary layer dynamics, the Grell cumulus convection scheme (Grell, 1993) for convective processes, the CLM4.5 land surface process module (Oleson et al., 2008; Stöckli et al., 2008) for terrestrial processes, and the CCM3 radiative transfer scheme (Zhang et al., 1998; Giorgi et al., 2012; Giorgi and Mearns, 1999) for simulating the radiative effects within the atmosphere.

2.3 Input data

The meteorological initial conditions for our model are sourced from the ERA-Interim reanalysis dataset (Dee, 2011), encompassing parameters such as temperature, humidity, potential height, and wind. These data are ingested every six hours to inform the model's meteorological boundary conditions, thereby constraining the simulated meteorological fields (Zhang et al., 2024). The model also receives average sea surface temperature data from the National Oceanic and Atmospheric Administration

https://doi.org/10.5194/egusphere-2025-608
Preprint. Discussion started: 25 March 2025

(NOAA) (Reynolds et al., 2002) on a weekly basis, while the chemical boundary conditions reflecting the climate state are derived from the time-varying outputs of the Global Chemical Transport Model (MOZART) (Hauglustaine et al., 1998; Horowitz et al., 2003). This model operates on a 6-hourly time resolution. The anthropogenic emission inventory is based on the MIX Asia emission inventory (Li et al., 2017), which offers a spatial resolution of 0.25° x0.25° . Within the scope of this paper, we utilize two distinct datasets for N_2O flux data: the Copernicus Atmosphere Monitoring Service (CAMS) (CAMS, 2023) and the Emission Database for Global Atmospheric Research (EDGAR) N_2O flux datasets (Crippa, 2024).

CAMS, which is operated by the European Centre for Medium-Range Weather Forecasts (ECMWF) on behalf of the European Commission, is one of the six services comprising the Copernicus program. The N_2O flux data for CAMS is derived using the atmospheric inversion framework PyVAR-N_2O. This framework relies on observations of N_2O mixing ratios to estimate the flux that best accounts for these observations, while being informed by a priori flux estimates. The CAMS Global Inversion Optimized Greenhouse Gas (GHG) fluxes and concentrations dataset encompasses net surface fluxes, model-level mixing ratios, and column average mixing ratios for CO_2, CH_4 and N_2O. These net fluxes encompass contributions from both the natural biosphere, such as vegetation and wetlands, as well as anthropogenic sources, including fossil fuel emissions and rice fields. The optimized N_2O flux data from CAMS are archived as NetCDF files, with each file containing a month's worth of time-varying flux data at a spatial resolution of 2.5° x 1.26° . Additionally, a three-dimensional N_2O concentration field, generated using the optimized flux data, is also saved in NetCDF format. Each monthly file includes 79 vertical layers of N_2O concentration data with a horizontal resolution of 2.5° x 1.26° , recorded every 3 hours. The CAMS N_2O concentration data serve as the initial and boundary conditions for model initialization, while the N_2O flux data are used as the emission input within the model to simulate N_2O emissions.

EDGAR is a comprehensive, independent global database that documents anthropogenic greenhouse gas emissions and air pollution worldwide. Utilizing international statistics and consistent IPCC methodologies, EDGAR offers independent emissions estimates, providing a valuable comparison to those reported by European member states or parties under the United Nations Framework Convention on Climate Change (UNFCCC). The database provides a grid of total national emissions at a global scale with a resolution of 0.1° x 0.1° , including annual, monthly, and hourly data. For this study, we have

https://doi.org/10.5194/egusphere-2025-608
Preprint. Discussion started: 25 March 2025

utilized EDGAR's monthly N_2O emission grid for 2020, categorized by sector, in units of kg/m² /s, with a spatial resolution of 0.1° x 0.1° . The sectors covered include: the power industry for electric and thermal power plants (both public and private), industrial combustion for manufacturing processes, small-scale non-industrial fixed combustion in buildings, transportation for mobile combustion sources (road, rail, ship and aviation), agricultural soils, crop residue burning, enteric fermentation, manure management, and agricultural indirect N_2O emissions. Additionally, it includes emissions from fuel production, fuel extraction (such as conversion and refining), industrial processes (e.g. cement, steel, aluminum, chemicals, solvents), and the waste industry, encompassing solid waste treatment and wastewater management. The 12-month emissions for each sector in 2020, as provided by EDGAR, were consolidated into a total flux file. This file was then input into the model as an alternative set of N_2O emissions for simulation purposes.

https://doi.org/10.5194/egusphere-2025-608
Preprint. Discussion started: 25 March 2025

2.4 Validation data

The World Greenhouse Gas Data Center (WDCGG) (Lan, 2023) is a World Data Center (WDC) operated by the Japan Meteorological Agency (JMA) under the Global Atmospheric Watch (GAW) program of the World Meteorological Organization (WMO). WDCGG collects, archives, and distributes data on greenhouse gases (e.g. CO_2, CH_4, CFCs, N_2O) and related gases (e.g. CO) from the atmosphere and other sources, provided by various contributors. In this study, data from six N_2O observation sites in WDCGG were utilized to validate the model simulation results. These sites include Anmyeon-do (AMY), Gosan (GSN), and Tae-ahn Peninsula (TAP) in the Republic of Korea, Ulaan Uul (UUM) in Mongolia, and Mt. Waliguan (WLG) and Lulin (LLN) in China. The N_2O concentration data from WDCGG encompass monthly data for the six sites, daily data for AMY and GSN, and hourly data for AMY and GSN. Both WLG and LLN are located on plateaus, while UUM is situated in a vast and sparsely populated area, less influenced by human activities, thus providing a better representation of natural N_2O concentrations. The AMY and GSN stations are near the ocean and are significantly affected by marine sources. The spatial distribution of these N_2O monitoring stations is depicted in Fig.1, and their latitude and longitude coordinates are listed in Table 1.

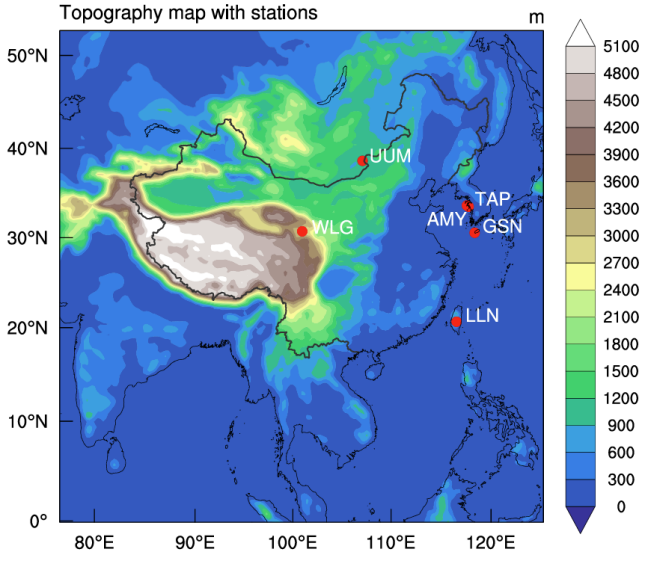

Figure 1. The model domain of the RegCM-Chem-YIBs model and location of WDCGG N_2O measurement sites.

https://doi.org/10.5194/egusphere-2025-608
Preprint. Discussion started: 25 March 2025

Table 1. Geographic information of the observation sites

Site	Abbreviation	Longitude(°E)	Latitude(°N)	Altitude(m)
Anmyeon-do	AMY	126.33	36.54	42
Gosan	GSN	126.16	33.29	71
Lulin	LLN	120.87	23.47	2862
Tae-ahn Peninsula	TAP	126.13	36.73	20
Ulaan Uul	UUM	111.08	44.44	992
Mt. Waliguan	WLG	100.90	36.29	3810

3 Results and discussion

3.1 Distribution characteristics of two different emissions

In this trial, we employed two distinct emission datasets: the CAMS net surface N_2O flux derived from ECMWF inversion and EDGAR's sectoral N_2O emission inventory. To facilitate a more direct comparison of emission differences between these two sources, we averaged the emissions at the grid points within the simulated region and compared the average monthly emissions for each month of 2020 between the two datasets (as shown in Fig.7). The analysis reveals that for the flux of EDGAR remains relatively stable throughout the year, with no significant seasonal variation. The average annual nitrification flux is 2.475×10^{-12} kg/m^2/s, with a fluctuation amplitude of 0.27 ppb. In contrast, the net flux from CAMS exhibits greater variability than the EDGAR, with a notable increase in flux during July, August, and September. The N_2O emission is comparatively lower in winter, with a fluctuation amplitude of 0.96 ppb. The average annual emission flux of nitrous oxide for CAMS is 3.965×10^{-12} kg/m^2/s, which is 1.6 times that of the EDGAR. The accounting of anthropogenic and natural sources of N_2O in China indicates that anthropogenic emissions in China for the year 2020 amount to 6.3×10^{-12} kg/m^2/s, while the combined natural and anthropogenic emissions total 7.5×10^{-12} kg/ m^2/s (Liang et al., 2024b). These figures are more aligned with the emission utilized in this study.

We have depicted the annually spatial distributions and zonally averaged N_2O fluxes for both datasets across the year in Fig.2. We selected January, April, July and October to represent the four seasons of spring, summer, autumn and winter to analyze the seasonal characteristics of N_2O, as shown in Fig.S1. As observed in Fig.2, within the study area, North China and the Ganges River basin in India exhibit elevated N_2O fluxes, surpassing 1.5×10^{-11} kg/m^2/s. Besides these two extensive regions with

https://doi.org/10.5194/egusphere-2025-608
Preprint. Discussion started: 25 March 2025

significant N_2O emissions, China and India also feature numerous localized areas with high N_2O emissions. This could be attributed to the intensive use of nitrogen fertilizers in these regions, as they are a primary source of N_2O from agricultural lands (Shengji Yan, 2022). Furthermore, urbanization can lead to reduced flow rates and dissolved oxygen levels, as well as increased nitrogen availability and denitrification processes, potentially contributing to higher concentrations and fluxes of N_2O (Chen et al., 2025). In contrast, Northwest China, the Tibetan Plateau, and Inner Mongolia are characterized by relatively lower N_2O emissions. This may be due to less agricultural intensification, reduced nitrogen fertilizer application, distinct climatic conditions and soil properties, and a more pristine and less polluted natural environment in these areas (Wang et al., 1998; Du et al., 2016). The pattern of high and low emission regions aligns with the findings of previous studies (Liang et al., 2024b; Zhou et al., 2014; Garg et al., 2011; Wang et al., 1998). It is noteworthy that in the CAMS flux distribution, the western Pacific region along China's coast displays a relatively pronounced negative N_2O flux during winter. This indicates that the ocean along China's coast acts as a weak sink for N_2O during late autumn and throughout winter and early spring. In summary, it is evident that the EDGAR datasets, with their higher resolution of 0.1°×0.1°, provide a more detailed distribution of N_2O in the target area compared to the CAMS flux data at 2.5°×2.5°. Despite the CAMS datasets being more accurate and closer to reality, they exhibit significant seasonal variations and fluctuations.

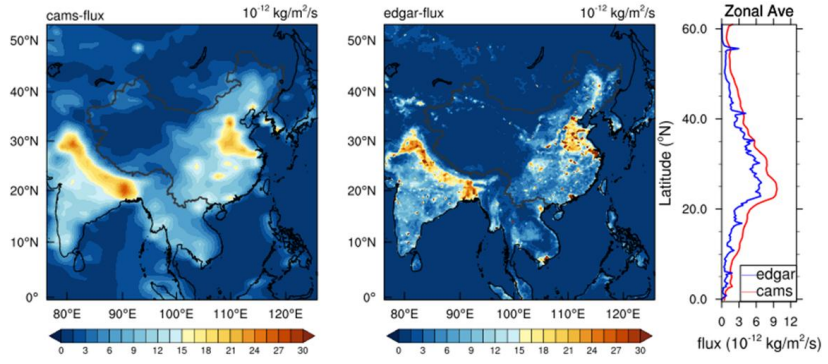

Figure 2. Comparison of annually averaged spatial distribution and zonal mean nitrous oxide flux between two datasets.

https://doi.org/10.5194/egusphere-2025-608
Preprint. Discussion started: 25 March 2025

3.2 Model evaluation

By comparing the model simulation results with the observations, we evaluated the performance of the model based on a number of meteorological factors, including air temperature (T), relative humidity (RH), and wind speed. As shown in Fig.3 and Fig.S2, as well as Table 2, the RegCM-Chem-YIBs model has successfully captured the spatial distribution and intensity of both temperature and specific humidity at the 500hPa, 850hPa, and 1000hPa pressure levels. Notably, the model's simulated correlation coefficient for wind at 500hPa height reached 0.95, indicating the precision of the model's simulation capabilities. The simulation correlation between the model and observational data for the middle and lower atmospheric layers is also significant, with values ranging from 0.36 to 0.44, as detailed in Table 2. Within these layers, the model's simulation of wind speed over the Qinghai-Tibet Plateau and sea areas is relatively accurate, and the wind direction is largely correctly predicted. Prior research (Xie et al., 2019; Xie et al., 2020; Xu et al., 2023; Xu et al., 2022; Ma et al., 2023a; Ma et al., 2023b; Zhang et al., 2024; Xie et al., 2024; Yin et al., 2015; Gao et al., 2023) has similarly validated the model's proficiency in accurately representing air quality, weather fields, and major greenhouse gases in Asia. When comparing the two distinct sources, it was observed that the meteorological field simulated using the CAMS flux model aligns more closely with observational outcomes. Given that CAMS flux data are derived from the inversion of model results, they are deemed more precise than the EDGAR emission inventories, especially under the dual constraints of observational and model-based accuracy. Furthermore, different models may exhibit varying sensitivities to emissions, which is contingent upon how chemical and physical processes are handled within the model framework. Models that exhibit heightened sensitivity to emissions may yield more precise simulation results under specific conditions.

https://doi.org/10.5194/egusphere-2025-608
Preprint. Discussion started: 25 March 2025

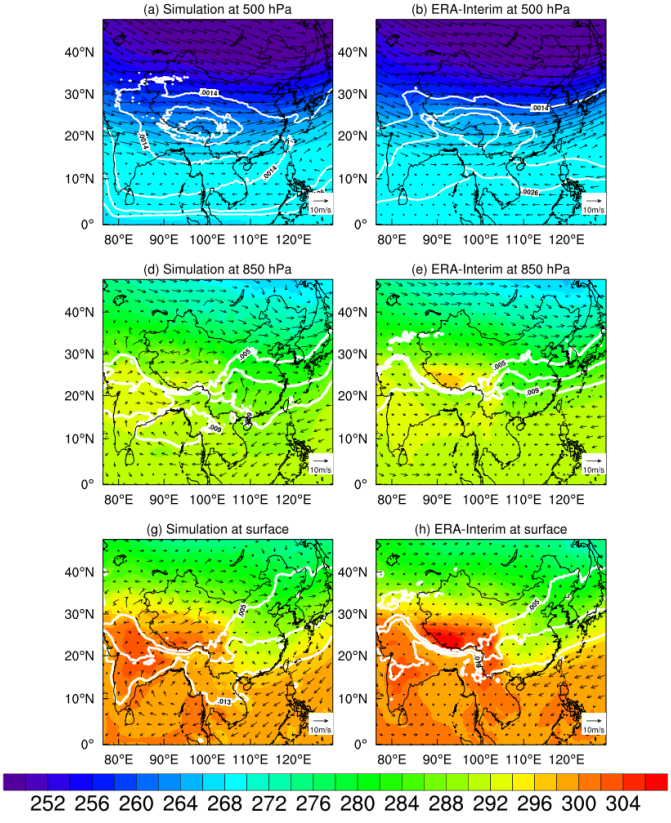

Figure 3. Annual average temperature (color-filled; units: K), specific humidity (contours; units: kg kg-1) and wind field (streamlines; units: m/s) at 500 hPa (a, b), 850 hPa (c, d) and surface (e, f) for the ERA-Interim reanalysis data (a, c, e) and model simulation (b, d, f). This is the result of the CAMS dataset.

Table 2. Statistical indicators for comparing model simulation results with reanalysis data Statistical characteristics of simulated (Sim) and observed (Obs) monthly N_2O mixing ratios at the seven stations

Factors	Altitude	[a]R	[b]R
Temperature (K)	500hPa	0.998	0.997
	850hPa	0.989	0.988
	1000hPa	0.988	0.988
Specific humidity (Kg Kg^{-1})	500hPa	0.854	0.831
	850hPa	0.985	0.983
	1000hPa	0.988	0.986
Wind speed (m/s)	500hPa	0.963	0.952
	850hPa	0.442	0.424
	1000hPa	0.363	0.368

([a]R indicates the correlation coefficient of CAMS, [b]R indicates the correlation coefficient of EDGAR.)

https://doi.org/10.5194/egusphere-2025-608
Preprint. Discussion started: 25 March 2025

Figure 4 juxtaposes the monthly average mixing ratios of N_2O at the six observation sites, as both observed and simulated by the model, with detailed statistical insights provided in Table 3. The figure reveals that the model's simulated N_2O concentrations closely match the observed values, particularly at the LLN station. Notably, the N_2O mixing ratios at TAP, AMY, and GSN exhibit pronounced seasonality, peaking in spring or summer and plummeting in winter. This pattern is attributed to higher air-sea fluxes during spring and summer, with the East China Sea and South China Sea regions serving as net sources of N_2O (Chen et al., 2021). At inland locations such as UUM and WLG, the simulated and observed N_2O concentrations follow a similar upward trend. However, the N_2O concentrations simulated with both sources exceed the observed concentrations, with those using EDGAR emissions being closer to the actual measurements. For the LLN site, the simulation outcomes from the two emissions are highly congruent, mirroring the observational data. The LLN site exhibits subdued seasonality, with N_2O concentrations being lower in summer and winter and slightly elevated in spring and autumn.

Based on the fitting results from the model simulations and observations at the six sites, as detailed in Table S1, the correlation coefficients for LLN, WLG, and UUM are exceptionally high. Generally, the simulation results using the CAMS emission source outperform those using EDGAR, with correlation coefficients ranging from 0.82 to 0.92. In contrast, the correlation for the other three coastal sites is comparatively low. This is likely due to the significant influence of marine environmental factors such as land and sea breezes, sea fog, and salt fog on meteorological conditions in coastal areas (Qiu and Fan, 2013). The complexity of these factors may contribute to the less accurate simulation outcomes in these regions. For these six sites, the discrepancy between the CAMS-calculated concentration values and the observed values is minimal, varying from -0.09% to 0.31%. Similarly, the deviation between the concentration values calculated by EDGAR and the observed values is also very small, ranging from -0.18% to 0.14%. Regarding the annual variation in simulated N_2O concentrations, UUM, WLG and LLN sites exhibit smaller fluctuations, while TAP, AMY and GSN sites display larger annual variations. In coastal regions, the sea-air exchange flux is substantial, and the transfer of N_2O from the ocean to the atmosphere is more dynamic, potentially leading to greater annual variability of N_2O at coastal sites (Wang et al., 2023).

https://doi.org/10.5194/egusphere-2025-608
Preprint. Discussion started: 25 March 2025

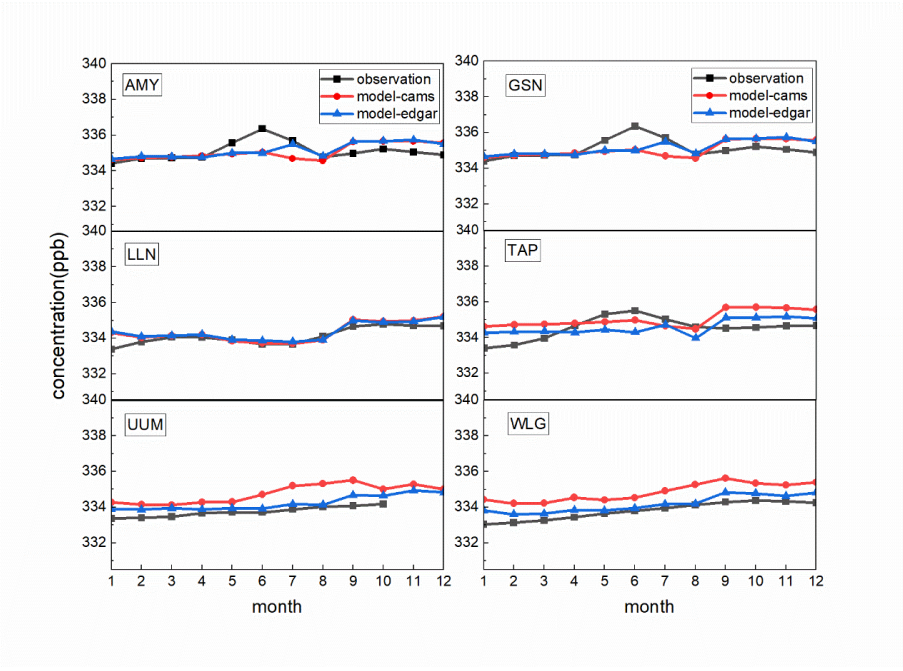

Figure 4. The monthly mean mixing ratio of nitrous oxide at the six sites observed and simulated by the model.

Table 3. Statistical characteristics of simulated (Sim) and observed (Obs) monthly N_2O mixing ratios at the seven stations Correlation coefficients and RMSE between the simulated results and the observed values for the two emission sources

Site	Mean					Annual amplitude			Standard deviation		
	Sim1	Sim2	Obs	Bias1	Bias2	Sim1	Sim2	Obs	Sim1	Sim2	Obs
AMY	335.06	335.16	335.09	-0.01	0.02	1.09	1.08	1.95	0.44	0.41	0.52
GSN	334.43	334.12	334.73	-0.09	-0.18	1.37	1.34	1.80	0.49	0.51	0.57
LLN	334.34	334.36	334.12	0.07	0.07	1.52	1.38	1.41	0.56	0.50	0.46
TAP	335.04	334.60	334.53	0.15	0.02	1.22	1.21	2.10	0.47	0.42	0.60
UUM	334.76	334.23	333.75	0.30	0.14	1.39	1.07	0.82	0.52	0.41	0.27
WLG	334.84	334.17	333.80	0.31	0.11	1.41	1.23	1.33	0.51	0.47	0.47

($Bias_1 = \frac{Sim_1 - Obs}{Obs} \times 100\%$, $Bias_2 = \frac{Sim_2 - Obs}{Obs} \times 100\%$. Subscript 1 represents CAMS flux and subscript 2 represents EDGAR flux. Sim1 represents the nitrous oxide mixing ratio modeled using CAMS flux, Sim2 represents the nitrous oxide mixing ratio modeled using EDGAR flux, the units of Sim1, 2 and Obs are ppb, the unit of Bias is %)

https://doi.org/10.5194/egusphere-2025-608
Preprint. Discussion started: 25 March 2025

3.3 Spatiotemporal distribution of N_2O

Figure 5 illustrates the spatial distribution of N_2O surface concentrations simulated using two different fluxes. In a similar vein, we utilize the months of January, April, July, and October to depict the seasonal fluctuation of nitrous oxide. In combination with Fig.S3, the surface N_2O concentration simulated by two different emissions exhibit a relatively consistent trend: from spring to winter, the concentrations initially decrease and then increase. The monthly average surface N_2O concentrations simulated by CAMS and EDGAR reach their lowest values in June, at 334.01 ppb and 333.79 ppb, respectively, and their highest values in December, at 335.42 ppb and 335.15 ppb, respectively. Regardless of the month, N_2O concentrations are high in central and eastern China, particularly in the North China Plain, Sichuan Basin, and the Ganges Valley in India. In contrast, the Tibetan Plateau, the Indian Ocean, and the South China Sea are characterized by low concentrations, aligning with the intensity of imported N_2O emissions. The North China Plain and Sichuan Basin are major agricultural regions in China, where extensive use of nitrogen fertilizers leads to increased N_2O emissions (Liang et al., 2024b; Shengji Yan, 2022). In China, in particular, the intensive scale development of agriculture to support 22% of the world's population has resulted in heavy nitrogen fertilizer usage, further boosting N_2O emissions. The central and eastern regions of China are densely populated and industrially advanced, with industrial emissions and municipal waste from these areas also contributing significantly to N_2O emissions (Bu et al., 2024; Luo et al., 2019).

The findings indicate that ground-level N_2O emissions significantly influence its atmospheric concentration, exhibiting a strong correlation. In the Qinghai-Tibet Plateau, the high altitude and low temperatures lead to reduced microbial activity, resulting in lower N_2O production. Additionally, the thin air at high altitudes contributes to the relatively low concentration of N_2O. In the Indian Ocean and the South China Sea, ocean dynamics primarily dictate N_2O levels. While the gas mainly originates from denitrification processes in seafloor sediments, the unique marine environment keeps its concentration

https://doi.org/10.5194/egusphere-2025-608
Preprint. Discussion started: 25 March 2025

relatively low (Craig and Gordon, 1963).

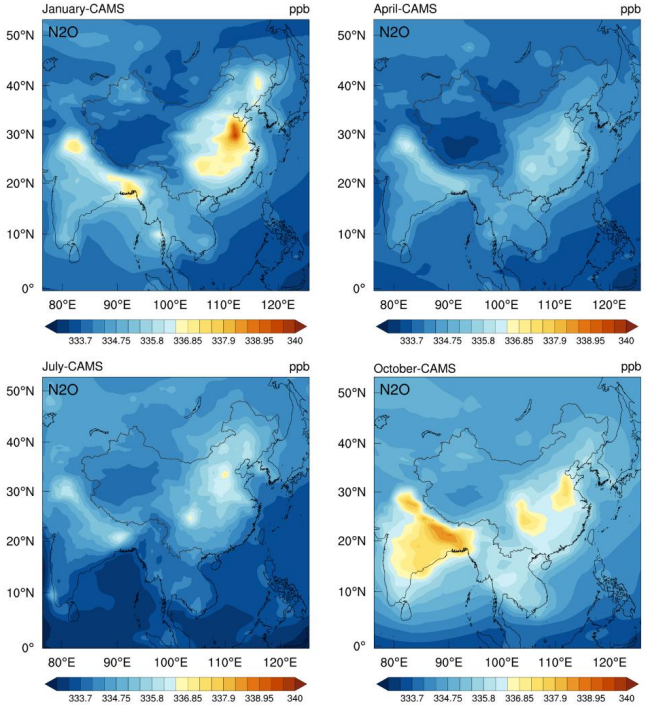

Figure 5. The distribution of the seasonal average ground-level N_2O concentration in 2020, as simulated by the CAMS datasets

We selected January, April, July and October to represent the four seasons of spring, summer, autumn and winter, respectively, to investigate the seasonal variation characteristics of the vertical distribution of N_2O (Fig.S4). Additionally, we obtained the annual vertical profile of nitrous oxide for the study period, depicted in Fig.6. According to Fig.6 and Fig.S4, regardless of whether using the CAMS flux or the EDGAR flux, N_2O is uniformly distributed at high concentrations in the middle and lower troposphere. From the upper troposphere to the lower stratosphere, the concentration of N_2O gradually decreases (Krysztofiak et al., 2023; Tsai et al., 2012). Overall, the concentration of N_2O at the same pressure height gradually decreases from the equator to the high latitudes of the northern hemisphere,

https://doi.org/10.5194/egusphere-2025-608
Preprint. Discussion started: 25 March 2025

such as in spring and autumn. However, in summer, the high-value area shifts northward to around 30° N latitude, with a relative low-value area in the troposphere over the equatorial region. In winter, the high-value area of the troposphere is near the latitude of 15°N. The RegCM-Chem-YIBs model used in this study extends up to 50hPa, covering the middle and lower stratosphere, but it does not include any N_2O loss processes. Therefore, future research should incorporate the atmospheric chemical sink of N_2O in the stratosphere so as to better study the vertical change trends of N_2O.

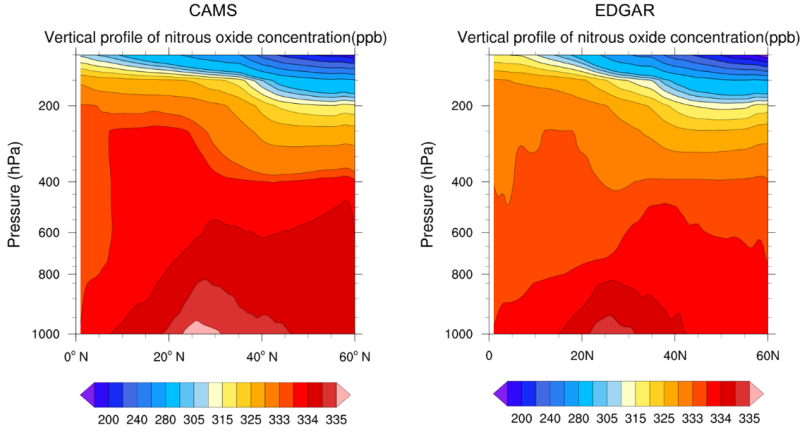

Figure 6. Vertical profiles of N_2O in 2020 from two emissions simulations.

3.4 Seasonality of ground N_2O concentrations

Our enhanced RegCM-Chem-YIBs model simulates the emission process of N_2O, as well as its advection, diffusion, and other transport processes in the atmosphere. The resulting concentration distribution of N_2O exhibits pronounced seasonality (Nevison et al., 2011; Yang et al., 2020; Jiang et al., 2007; Sun et al., 2024; Liao et al., 2004), primarily due to the combined effects of ground-level emissions, atmospheric transport processes, and stratosphere-troposphere gas exchange. We utilized two distinct sets of emissions to investigate their impacts on N_2O concentrations, as illustrated in Fig.7. The EDGAR emission inventory indicates that N_2O emissions show minimal variation throughout the 12 months of 2020, with only slight fluctuations. The monthly average changes in N_2O flux data derived from CAMS reanalysis are slightly more pronounced than those from EDGAR, yet there is no significant seasonal fluctuation. However, the monthly average concentration of surface N_2O obtained from these two sources

https://doi.org/10.5194/egusphere-2025-608
Preprint. Discussion started: 25 March 2025

display the same variation trend: the concentration reaches its lowest value in June and its highest value in December, exhibiting clear seasonality, which aligns with the average seasonal variation observed at Mt. Waliguan (Liang et al., 2024a). This suggests that in the studied Northern Hemisphere region, higher emissions correspond to higher surface N_2O concentrations. However, the seasonal relationship between surface N_2O concentration and surface emissions is relatively weak, while the seasonal relationship with atmospheric transport is more significant. Nevertheless, the seasonal characteristics of N_2O over oceans and land differ, with distinct dominant influencing factors (Jiang et al., 2007; Sun et al., 2024; Liao et al., 2004), necessitating further analysis specific to these regions.

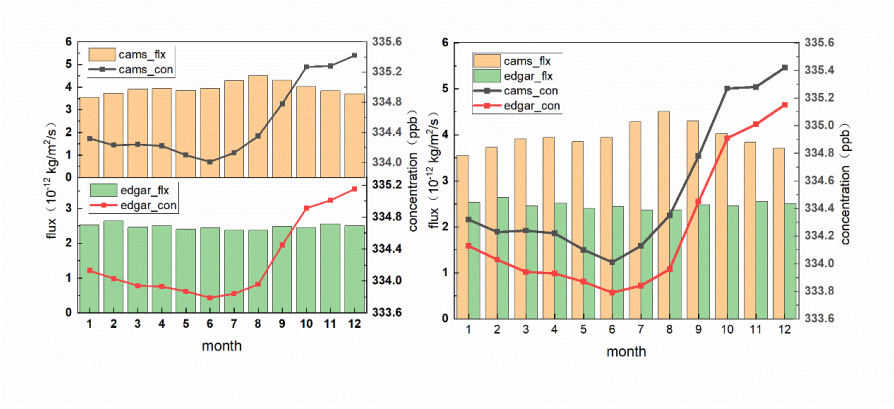

Figure 7. Plots of the monthly average emissions of the two emissions and their corresponding monthly mean N_2O surface concentrations

4 Summary and conclusions

In this study, the RegCM-Chem-YIBs model was improved to incorporate N_2O as a species, allowing for the simulation of its emission, transport, and diffusion processes in the atmosphere, thereby obtaining the distribution of N_2O. We employed this improved model to simulate N_2O in East Asia and most parts of South and Southeast Asia in 2020 utilizing two different emissions: the CAMS model inversion flux and the EDGAR emission inventory. Subsequently, we verify the model's ability to simulate the spatial and temporal distribution of N_2O in the target region, and evaluate the model's performance using the WDCGG ground observation data. Thereafter, the spatiotemporal distribution of N_2O in the model output were analyzed. Finally, the causes of N_2O seasonality were investigated using

https://doi.org/10.5194/egusphere-2025-608
Preprint. Discussion started: 25 March 2025

the simulations from the two emissions datasets.

The research indicates that between spring and winter, the average surface N_2O in the study area decreases initially, then rises again. The monthly average surface N_2O concentration simulated by CAMS and EDGAR reached their lowest values in June, at 334.01 ppb and 333.79 ppb, respectively, and their highest values in December, at 335.42 ppb and 335.15 ppb, respectively. Regardless of the month, the concentrations of N_2O are high in central and eastern China, particularly in the North China Plain, Sichuan Basin and Ganges valley of India. In contrast, the Tibetan Plateau, the Indian Ocean, the South China Sea and other sea areas are in a state of low concentration, which is consistent with the intensity of the input N_2O emissions. In the vertical profile, N_2O is uniformly distributed at high concentrations in the middle and lower troposphere. From the upper troposphere to the lower stratosphere. The concentration of N_2O is markedly higher near the ground and shows a gradual reduction with height. On the whole, the mixing ratio of N_2O at the same pressure level gradually decreases from the equator to the higher latitudes in the northern Hemisphere. By comparing the simulation results of two different emissions, it is evident that the seasonal relationship between surface N_2O concentration and surface emission is relatively weak. The model used in this study does not include the stratospheric chemical sink of N_2O, so the observed seasonality is primarily related to the atmospheric transport of N_2O. For this model, the temporal and spatial distribution characteristics of N_2O presented by the simulation results of two emissions are largely consistent, with the results being more accurate when using the CAMS emission.

In summary, this study improves a reliable high-resolution regional climate-chemistry-ecology model. This enhanced model can be used to develop a high-resolution inverse modeling system for N_2O in future studies, as well as to investigate its climate and environmental impacts. Additionally, there is still potential for further refinement in subsequent research. First, model may overestimate the actual concentration of N_2O in the atmosphere because they do not account for loss processes, such as photolysis and chemical reactions, which reduce N_2O. The photolysis of N_2O in the stratosphere is a significant chemical sink, and the material exchange (STE) between the stratosphere and the troposphere greatly influences the distribution of N_2O in both the troposphere and at the surface (Ray et al., 2019; Jiang et al., 2007). This exchange contributes significantly to the seasonal cycle of N_2O in the troposphere of the Northern Hemisphere. Secondly, it is essential to include heterogeneous N_2O in the calculation of

https://doi.org/10.5194/egusphere-2025-608
Preprint. Discussion started: 25 March 2025

longwave radiation This would enable the estimation of the N_2O radiative forcing, providing a more accurate evaluation of its radiative and climate effects. Finally, we aim to further optimize N_2O flux, accurately describing its sources and sinks. These improvements will help refine the RegCM-Chem-YIBs model, allowing it to more precisely predict N_2O emissions and distribution, thereby offering stronger support for global climate change mitigation and ozone layer protection.

Code and data availability

The input data and source code for RegCM-Chem-YIBs have been archived on Zenodo at https://doi.org/10.5281/zenodo.15043206 (Zeng et al., 2025). Data used in this study are listed as follows: the European Centre for Medium Range Weather Forecasts (ECMWF) ERA-Interim reanalysis are provided at https://doi.org/10.24381/cds.f2f5241d (Dee, 2011), the Copernicus Atmosphere Monitoring Service(CAMS) N_2O fluxes are available at https://ads.atmosphere.copernicus.eu/datasets/cams-global-greenhouse-gas-inversion?tab=overview (CAMS, 2023), the EDGAR's N_2O emission inventory is provided at https://edgar.jrc.ec.europa.eu/dataset_ghg2024#p4 (Crippa, 2024) and the World Data Centre for Greenhouse Gases (WDCGG) N_2O observation data are accessed at https://doi.org/10.15138/53g1-x417 (Lan, 2023).

Author contributions

TW and XZ designed this study. XZ modified the model, performed the experiments, and drafted the manuscript. TW revised the manuscript, and all authors contributed to the review and editing of the manuscript.

Competing interests

The corresponding author has stated that all the authors have no conflicts of interest.

Disclaimer

Publisher's note: Copernicus Publications remains neutral about jurisdictional claims in published maps and institutional affiliations.

https://doi.org/10.5194/egusphere-2025-608
Preprint. Discussion started: 25 March 2025

Acknowledgments

This work was supported by the National Key Basic Research Development Program of China (2024YFC3711905) and the National Natural Science Foundation of China (42477103).

References

Beusen, A. H. W., Bouwman, A. F., Van Beek, L. P. H., Mogollón, J. M., and Middelburg, J. J.: Global riverine N and P transport to ocean increased during the 20th century despite increased retention along the aquatic continuum, Biogeosciences, 13, 2441-2451, 10.5194/bg-13-2441-2016, 2016.

Bi, Y., Xu, L., and Zhou, R.: Simulation of influence of N_2O's increase on atmospheric environment and comparison with the influences of methane and stratospheric water vapor, CHINESE JOURNAL OF GEOPHYSICS, 56, 38-46, 10.6038/cjg20130104, 2013.

Blagodatsky, S., Grote, R., Kiese, R., Werner, C., and Butterbach-Bahl, K.: Modelling of microbial carbon and nitrogen turnover in soil with special emphasis on N-trace gases emission, Plant and Soil, 346, 297-330, 10.1007/s11104-011-0821-z, 2011.

Bu, M., Xi, W., Wang, Y., and Wang, G.: Scenario-Based Modeling of Agricultural Nitrous Oxide Emissions in China, Agriculture, 14, 10.3390/agriculture14112074, 2024.

Chen, X., Wang, J., Liu, J., Zhang, S., Gao, H., and Xia, X.: Unveiling riverine N(2)O dynamics along urbanization gradients by integrating hydrological, biogeochemical and microbial processes, Water Res, 268, 122620, 10.1016/j.watres.2024.122620, 2025.

Chen, X., Ma, X., Gu, X., Liu, S., Song, G., Jin, H., and Zhang, G.: Seasonal and spatial variations of N_2O distribution and emission in the East China Sea and South Yellow Sea, Science of The Total Environment, 775, 10.1016/j.scitotenv.2021.145715, 2021.

Craig, H. and Gordon, L. I.: Nitrous oxide in the ocean and the marine atmosphere, Geochimica et Cosmochimica Acta, 27, 949-955, 10.1016/0016-7037(63)90104-2, 1963.

Crippa, M., Guizzardi, D., Pagani, F., Banja, M., Muntean, M., Schaaf, E., Monforti-Ferrario, F., Becker, W.E., Quadrelli, R., Risquez Martin, A., Taghavi-Moharamli, P., Köykkä, J., Grassi, G., Rossi, S., Melo, J., Oom, D., Branco, A., San-Miguel, J., Manca, G., Pisoni, E., Vignati, E. and Pekar, F.: GHG emissions of all world countries, Publications Office of the European Union, Luxembourg, 10.2760/953332, 2024.

De Sisto, M., Somes, C., Landolfi, A., and MacDougall, A. H.: Projecting atmospheric N_2O rise until the end of the 21st century: an Earth System Model study, Environmental Research Letters, 19, 10.1088/1748-9326/ad8c6c, 2024.

Dee, D.P., Uppala, S.M., Simmons, A.J., Berrisford, P., Poli, P., Kobayashi, S., Andrae, U., Balmaseda, M.A., Balsamo, G., Bauer, P., Bechtold, P., Beljaars, A.C.M., van de Berg, L., Bidlot, J., Bormann, N., Delsol, C., Dragani, R., Fuentes, M., Geer, A.J., Haimberger, L., Healy, S.B., Hersbach, H., Hólm, E.V., Isaksen, L., Kållberg, P., Köhler, M., Matricardi, M., McNally, A.P., Monge-Sanz, B.M., Morcrette, J.-.-J., Park, B.-.-K., Peubey, C., de Rosnay, P., Tavolato, C., Thépaut, J.-.-N. and Vitart, F. ERA-Interim global atmospheric reanalysis. Copernicus Climate Change Service (C3S) Climate Data Store (CDS): https://doi.org/10.24381/cds.f2f5241d , last access: 25 October 2024.

Du, Y., Zhou, G., Guo, X., and Li, J.: Response of N_2O emission flux to soil temperature and moisture in alpine meadow on Qinghai-Tibetan Plateau, Grassland and Turf, 36, 55-59,

https://doi.org/10.5194/egusphere-2025-608
Preprint. Discussion started: 25 March 2025

10.13817/j.cnki.cyycp.2016.01.010, 2016.

Gao, L., Wang, T., Ren, X., Ma, D., Qu, Y., and Wu, H.: Mechanism of persistent heavy $PM_{2.5}$ pollution over the Beijing-Tianjin-Hebei region of China: A combination of aerosol radiative effect and atmospheric quasi-biweekly oscillation, Atmospheric Environment, 303, 10.1016/j.atmosenv.2023.119751, 2023.

Garg, A., Shukla, P. R., and Upadhyay, J.: N_2O emissions of India: an assessment of temporal, regional and sector trends, Climatic Change, 110, 755-782, 10.1007/s10584-011-0094-9, 2011.

Geneva, W.: Executive Summary. Scientific Assessment of Ozone Depletion: 2022, GAW Report, WMO,No. 278, 56 pp. 2022.

Giorgi, F. and Mearns, L. O.: Introduction to special section: Regional Climate Modeling Revisited, Journal of Geophysical Research: Atmospheres, 104, 6335-6352, 10.1029/98jd02072, 1999.

Giorgi, F., Coppola, E., Solmon, F., Mariotti, L., Sylla, M. B., Bi, X., Elguindi, N., Diro, G. T., Nair, V., Giuliani, G., Turuncoglu, U. U., Cozzini, S., Güttler, I., O'Brien, T. A., Tawfik, A. B., Shalaby, A., Zakey, A. S., Steiner, A. L., Stordal, F., Sloan, L. C., and Brankovic, C.: RegCM4: model description and preliminary tests over multiple CORDEX domains, Climate Research, 52, 7-29, 10.3354/cr01018, 2012.

Grant, R. F., Goulden, M. L., Wofsy, S. C., and Berry, J. A.: Carbon and energy exchange by a black spruce-moss ecosystem under changing climate: Testing the mathematical model ecosys with data from the BOREAS experiment, Journal of Geophysical Research: Atmospheres, 106, 33605-33621, 10.1029/2001jd900064, 2001.

Grell, G. A.: Prognostic Evaluation of Assumptions Used by Cumulus Parameterizations, Monthly Weather Review, 121, 764-787, 10.1175/1520-0493(1993)121<0764:Peoaub>2.0.Co;2, 1993.

Hansen, S., Jensen, H. E., Nielsen, N. E., and Svendsen, H.: Simulation of nitrogen dynamics and biomass production in winter wheat using the Danish simulation model DAISY, Fertilizer Research, 27, 245-259, 10.1007/bf01051131, 1991.

Hauglustaine, D. A., Brasseur, G. P., Walters, S., Rasch, P. J., Müller, J. F., Emmons, L. K., and Carroll, M. A.: MOZART, a global chemical transport model for ozone and related chemical tracers: 2. Model results and evaluation, Journal of Geophysical Research: Atmospheres, 103, 28291-28335, 10.1029/98jd02398, 1998.

Holtslag, A. A. M., De Bruijn, E. I. F., and Pan, H. L.: A High Resolution Air Mass Transformation Model for Short-Range Weather Forecasting, Monthly Weather Review, 118, 1561-1575, 10.1175/1520-0493(1990)118<1561:Ahramt>2.0.Co;2, 1990.

Horowitz, L. W., Walters, S., Mauzerall, D. L., Emmons, L. K., Rasch, P. J., Granier, C., Tie, X., Lamarque, J. F., Schultz, M. G., Tyndall, G. S., Orlando, J. J., and Brasseur, G. P.: A global simulation of tropospheric ozone and related tracers: Description and evaluation of MOZART, version 2, Journal of Geophysical Research: Atmospheres, 108, 10.1029/2002jd002853, 2003.

Idowu, S. O., Schmidpeter, R., Capaldi, N., Zu, L., Del Baldo, M., and Abreu, R.: Encyclopedia of Sustainable Management, 10.1007/978-3-031-25984-5, 2023.

Jiang, X., Ku, W. L., Shia, R. L., Li, Q., Elkins, J. W., Prinn, R. G., and Yung, Y. L.: Seasonal cycle of N2O: Analysis of data, Global Biogeochemical Cycles, 21, 10.1029/2006gb002691, 2007.

Krysztofiak, G., Catoire, V., Dudok de Wit, T., Kinnison, D. E., Ravishankara, A. R., Brocchi, V., Atlas, E., Bozem, H., Commane, R., D'Amato, F., Daube, B., Diskin, G. S., Engel, A., Friedl-Vallon, F., Hintsa, E., Hurst, D. F., Hoor, P., Jegou, F., Jucks, K. W., Kleinböhl, A., Küllmann, H., Kort, E. A., McKain, K., Moore, F. L., Obersteiner, F., Ramos, Y. G., Schuck, T., Toon, G. C., Viciani, S., Wetzel,

https://doi.org/10.5194/egusphere-2025-608
Preprint. Discussion started: 25 March 2025

G., Williams, J., and Wofsy, S. C.: N_2O Temporal Variability from the Middle Troposphere to the Middle Stratosphere Based on Airborne and Balloon-Borne Observations during the Period 1987–2018, Atmosphere, 14, 10.3390/atmos14030585, 2023.

Lan, X.: Atmospheric Nitrous Oxide Dry Air Mole Fractions from the NOAA GML Carbon Cycle Cooperative Global Air Sampling Network, 1997-2022: https://doi.org/10.15138/53g1-x417 , last access: 15 May 2024.

Li, M., Zhang, Q., Kurokawa, J.-i., Woo, J.-H., He, K., Lu, Z., Ohara, T., Song, Y., Streets, D. G., Carmichael, G. R., Cheng, Y., Hong, C., Huo, H., Jiang, X., Kang, S., Liu, F., Su, H., and Zheng, B.: MIX: a mosaic Asian anthropogenic emission inventory under the international collaboration framework of the MICS-Asia and HTAP, Atmospheric Chemistry and Physics, 17, 935-963, 10.5194/acp-17-935-2017, 2017.

Liang, M., Fang, S., Liu, L., Zhang, Y., Wang, J., Liu, S., Wang, H., and Deng, L.: Variation characteristics of nitrous oxide concentration at Wari global background station in 2001~2018, Scientia Sinica(Terrae), 54, 97-109, 2024a.

Liang, M., Zhou, Z., Ren, P., Xiao, H., Xu, R., Hu, Z., Piao, S., Tian, H., Tong, Q., Zhou, F., Wei, J., and Yuan, W.: Four decades of full-scale nitrous oxide emission inventory in China, Natl Sci Rev, 11, nwad285, 10.1093/nsr/nwad285, 2024b.

Liao, T., Camp, C. D., and Yung, Y. L.: The seasonal cycle of N_2O, Geophysical Research Letters, 31, 10.1029/2004gl020345, 2004.

Luo, Z., Lam, S. K., Fu, H., Hu, S., and Chen, D.: Temporal and spatial evolution of nitrous oxide emissions in China: Assessment, strategy and recommendation, Journal of Cleaner Production, 223, 360-367, 10.1016/j.jclepro.2019.03.134, 2019.

Ma, D., Wang, T., Wu, H., Qu, Y., Liu, J., Liu, J., Li, S., Zhuang, B., Li, M., and Xie, M.: The effect of anthropogenic emission, meteorological factors, and carbon dioxide on the surface ozone increase in China from 2008 to 2018 during the East Asia summer monsoon season, Atmospheric Chemistry and Physics, 23, 6525-6544, 10.5194/acp-23-6525-2023, 2023a.

Ma, D., Wang, T., Xu, B., Song, R., Gao, L., Chen, H., Ren, X., Li, S., Zhuang, B., Li, M., Xie, M., and Saikawa, E.: The mutual interactions among ozone, fine particulate matter, and carbon dioxide on summer monsoon climate in East Asia, Atmospheric Environment, 299, 10.1016/j.atmosenv.2023.119668, 2023b.

Ma, P., Xiong, X., Chen, L., Tao, M., Chen, H., Zhang, Y., Zhang, L., Li, Q., Zhou, C., Chen, C., Zhang, L., Weng, G., and Wang, Z.: Temporal and Spatial Characteristics of Nitrous Oxide Concentration in China, Spectroscopy and Spectral Analysis, 41, 20-24, 10.3964/j.issn.1000-0593(2021)01-0020-05, 2021.

MacLeod, M., Hasan, M.R., Robb, D.H.F. & Mamun-Ur-Rashid, M. : Quantifying and mitigating greenhouse gas emissions from global aquaculture., FAO, Rome, ISBN 978-92-5-131992-5, 2019.

McElroy, M. B. and McConnell, J. C.: Nitrous Oxide: A Natural Source of Stratospheric NO, Journal of the Atmospheric Sciences, 28, 1095-1098, 10.1175/1520-0469(1971)028<1095:Noanso>2.0.Co;2, 1971.

CAMS: CAMS global inversion-optimised greenhouse gas fluxes and concentrations, https://ads.atmosphere.copernicus.eu/datasets/cams-global-greenhouse-gas-inversion?tab=overview , last access: 16 March 2024.

Nevison, C. D., Dlugokencky, E., Dutton, G., Elkins, J. W., Fraser, P., Hall, B., Krummel, P. B., Langenfelds, R. L., O'Doherty, S., Prinn, R. G., Steele, L. P., and Weiss, R. F.: Exploring causes of

https://doi.org/10.5194/egusphere-2025-608
Preprint. Discussion started: 25 March 2025

interannual variability in the seasonal cycles of tropospheric nitrous oxide, Atmospheric Chemistry and Physics, 11, 3713-3730, 10.5194/acp-11-3713-2011, 2011.

Nielsen, S. N., Anastácio, P. M., Frias, A. F., and Marques, J. C.: CRISP-crayfish rice integrated system of production. 5. Simulation of nitrogen dynamics, Ecological Modelling, 123, 41-52, 10.1016/s0304-3800(99)00166-0, 1999.

THE NOAA ANNUAL GREENHOUSE GAS INDEX (AGGI): https://gml.noaa.gov/aggi/aggi.html , last access: 15 October 2024.

Oleson, K. W., Niu, G. Y., Yang, Z. L., Lawrence, D. M., Thornton, P. E., Lawrence, P. J., Stöckli, R., Dickinson, R. E., Bonan, G. B., Levis, S., Dai, A., and Qian, T.: Improvements to the Community Land Model and their impact on the hydrological cycle, Journal of Geophysical Research: Biogeosciences, 113, 10.1029/2007jg000563, 2008.

Parton, W. J., Mosier, A. R., Ojima, D. S., Valentine, D. W., Schimel, D. S., Weier, K., and Kulmala, A. E.: Generalized model for N2 and N2O production from nitrification and denitrification, Global Biogeochemical Cycles, 10, 401-412, 10.1029/96gb01455, 1996.

Prather, M. J., Hsu, J., DeLuca, N. M., Jackman, C. H., Oman, L. D., Douglass, A. R., Fleming, E. L., Strahan, S. E., Steenrod, S. D., Sovde, O. A., Isaksen, I. S., Froidevaux, L., and Funke, B.: Measuring and modeling the lifetime of nitrous oxide including its variability, J Geophys Res Atmos, 120, 5693-5705, 10.1002/2015JD023267, 2015.

Qiu, X. and Fan, S.: Progress of Sea-Land Breeze Study and the Characteristics of Sea-Land Breeze in Three Coastal Areas in China, Meteorological Monthly, 39(2): 186-193. DOI: 10.7519/j.issn.1000-0526.2013.02.007., 2013.

Ravishankara, A. R., Daniel, J. S., and Portmann, R. W.: Nitrous oxide (N_2O): the dominant ozone-depleting substance emitted in the 21st century, Science, 326, 123-125, 10.1126/science.1176985, 2009.

Ray, E. A., Portmann, R. W., Yu, P., Daniel, J., Montzka, S. A., Dutton, G. S., Hall, B. D., Moore, F. L., and Rosenlof, K. H.: The influence of the stratospheric Quasi-Biennial Oscillation on trace gas levels at the Earth's surface, Nature Geoscience, 13, 22-27, 10.1038/s41561-019-0507-3, 2019.

Reynolds, R. W., Rayner, N. A., Smith, T. M., Stokes, D. C., and Wang, W.: An Improved In Situ and Satellite SST Analysis for Climate, Journal of Climate, 15, 1609-1625, 10.1175/1520-0442(2002)015<1609:Aiisas>2.0.Co;2, 2002.

Shalaby, A., Zakey, A. S., Tawfik, A. B., Solmon, F., Giorgi, F., Stordal, F., Sillman, S., Zaveri, R. A., and Steiner, A. L.: Implementation and evaluation of online gas-phase chemistry within a regional climate model (RegCM-CHEM4), Geoscientific Model Development, 5, 741-760, 10.5194/gmd-5-741-2012, 2012.

Shengji Yan, Z. S., Aixing Deng, Weijian Zhang: Spatiotemporal Characteristics and Reduction Approaches of Farmland N_2O Emission in China, Crops, 1-8, 10.16035/j.issn.1001-7283.2022.03.001, 2022.

Stange, F., Butterbach-Bahl, K., Papen, H., Zechmeister-Boltenstern, S., Li, C., and Aber, J.: A process-oriented model of N_2O and NO emissions from forest soils: 2. Sensitivity analysis and validation, Journal of Geophysical Research: Atmospheres, 105, 4385-4398, 10.1029/1999jd900948, 2000.

Stöckli, R., Lawrence, D. M., Niu, G. Y., Oleson, K. W., Thornton, P. E., Yang, Z. L., Bonan, G. B., Denning, A. S., and Running, S. W.: Use of FLUXNET in the Community Land Model development, Journal of Geophysical Research: Biogeosciences, 113, 10.1029/2007jg000562, 2008.

Sun, Q., Joos, F., Lienert, S., Berthet, S., Carroll, D., Gong, C., Ito, A., Jain, A. K., Kou-Giesbrecht, S.,

https://doi.org/10.5194/egusphere-2025-608
Preprint. Discussion started: 25 March 2025

Landolfi, A., Manizza, M., Pan, N., Prather, M., Regnier, P., Resplandy, L., Séférian, R., Shi, H., Suntharalingam, P., Thompson, R. L., Tian, H., Vuichard, N., Zaehle, S., and Zhu, Q.: The Modeled Seasonal Cycles of Surface N_2O Fluxes and Atmospheric N_2O, Global Biogeochemical Cycles, 38, 10.1029/2023gb008010, 2024.

Tian, H., Chen, G., Lu, C., Xu, X., Ren, W., Banger, K., Zhang, B., Tao, B., Pan, S., Liu, M., and Zhang, C.: Global land-atmosphere exchange of methane and nitrous oxide: magnitude and spatiotemporal patterns, Biogeosciences Discuss., 10, 19811-19865, 10.5194/bgd-10-19811-2013, 2013.

Tian, H., Xu, R., Canadell, J. G., Thompson, R. L., Winiwarter, W., Suntharalingam, P., Davidson, E. A., Ciais, P., Jackson, R. B., Janssens-Maenhout, G., Prather, M. J., Regnier, P., Pan, N., Pan, S., Peters, G. P., Shi, H., Tubiello, F. N., Zaehle, S., Zhou, F., Arneth, A., Battaglia, G., Berthet, S., Bopp, L., Bouwman, A. F., Buitenhuis, E. T., Chang, J., Chipperfield, M. P., Dangal, S. R. S., Dlugokencky, E., Elkins, J. W., Eyre, B. D., Fu, B., Hall, B., Ito, A., Joos, F., Krummel, P. B., Landolfi, A., Laruelle, G. G., Lauerwald, R., Li, W., Lienert, S., Maavara, T., MacLeod, M., Millet, D. B., Olin, S., Patra, P. K., Prinn, R. G., Raymond, P. A., Ruiz, D. J., van der Werf, G. R., Vuichard, N., Wang, J., Weiss, R. F., Wells, K. C., Wilson, C., Yang, J., and Yao, Y.: A comprehensive quantification of global nitrous oxide sources and sinks, Nature, 586, 248-256, 10.1038/s41586-020-2780-0, 2020.

Tsai, T. R., Rose, R. A., Weidmann, D., and Wysocki, G.: Atmospheric vertical profiles of O_3, N_2O, CH_4, CCl_2F_2, and H_2O retrieved from external-cavity quantum-cascade laser heterodyne radiometer measurements, Appl Opt, 51, 8779-8792, 10.1364/AO.51.008779, 2012.

UNEP: Drawing Down N_2O To Protect Climate and the Ozone Layer. A UNEP Synthesis Report, United Nations Environment Programme (UNEP), Nairobi, Kenya, ISBN: 978-92-807-3358-7, 2013.

Wang, G., Du, R., Wang, Y., Liu, G., Wang, Y., Chen, Z., and Lu, D.: Characteristics o f N_2O and CH_4 Fluxes and Their Seasonal Variations From Inner Mongolia G rassland, Acta Agrestia Sinica, 6, 306-311, 10.11733/j.issn.1007-0435.1998.04.010, 1998.

Wang, Z., Gu, T., Wen, Y., Cui, X., Jia, D., and Sun, J.: Distributions, sources, and air-sea fluxes of nitrous oxide in Bohai Bay, China, Frontiers in Marine Science, 10, 10.3389/fmars.2023.1105016, 2023.

Weber, J., Keeble, J., Abraham, N. L., Beerling, D. J., and Martin, M. V.: Global agricultural N2O emission reduction strategies deliver climate benefits with minimal impact on stratospheric O3 recovery, npj Climate and Atmospheric Science, 7, 10.1038/s41612-024-00678-2, 2024.

WMO: The State of Greenhouse Gases in the Atmosphere Based on Global Observations through 2022, https://library.wmo.int/idurl/4/68532 , last access: 6 June 2024.

Xie, N., Wang, T., Xie, X., Yue, X., Giorgi, F., Zhang, Q., Ma, D., Song, R., Xu, B., Li, S., Zhuang, B., Li, M., Xie, M., Andreeva Kilifarska, N., Gadzhev, G., and Dimitrova, R.: The regional climate–chemistry–ecology coupling model RegCM-Chem (v4.6)–YIBs (v1.0): development and application, Geoscientific Model Development, 17, 3259-3277, 10.5194/gmd-17-3259-2024, 2024.

Xie, X., Wang, T., Yue, X., Li, S., Zhuang, B., and Wang, M.: Effects of atmospheric aerosols on terrestrial carbon fluxes and CO_2 concentrations in China, Atmospheric Research, 237, 10.1016/j.atmosres.2020.104859, 2020.

Xie, X., Wang, T., Yue, X., Li, S., Zhuang, B., Wang, M., and Yang, X.: Numerical modeling of ozone damage to plants and its effects on atmospheric CO_2 in China, Atmospheric Environment, 217, 10.1016/j.atmosenv.2019.116970, 2019.

Xu, B., Wang, T., Ma, D., Song, R., Zhang, M., Gao, L., Li, S., Zhuang, B., Li, M., and Xie, M.: Impacts of regional emission reduction and global climate change on air quality and temperature to attain carbon neutrality in China, Atmospheric Research, 279, 10.1016/j.atmosres.2022.106384, 2022.

https://doi.org/10.5194/egusphere-2025-608
Preprint. Discussion started: 25 March 2025

654 Xu, B., Wang, T., Gao, L., Ma, D., Song, R., Zhao, J., Yang, X., Li, S., Zhuang, B., Li, M., and Xie, M.:
655 Impacts of meteorological factors and ozone variation on crop yields in China concerning carbon
656 neutrality objectives in 2060, Environ Pollut, 317, 120715, 10.1016/j.envpol.2022.120715, 2023.
657 Yang, S., Chang, B. X., Warner, M. J., Weber, T. S., Bourbonnais, A. M., Santoro, A. E., Kock, A.,
658 Sonnerup, R. E., Bullister, J. L., Wilson, S. T., and Bianchi, D.: Global reconstruction reduces the
659 uncertainty of oceanic nitrous oxide emissions and reveals a vigorous seasonal cycle, Proc Natl
660 Acad Sci U S A, 117, 11954-11960, 10.1073/pnas.1921914117, 2020.
661 Yin, C., Wang, T., Solmon, F., Mallet, M., Jiang, F., Li, S., and Zhuang, B.: Assessment of direct radiative
662 forcing due to secondary organic aerosol over China with a regional climate model, Tellus B:
663 Chemical and Physical Meteorology, 67, 10.3402/tellusb.v67.24634, 2015.
664 Yue, X. and Unger, N.: The Yale Interactive terrestrial Biosphere model version 1.0: description,
665 evaluation and implementation into NASA GISS ModelE2, Geoscientific Model Development, 8,
666 2399-2417, 10.5194/gmd-8-2399-2015, 2015.
667 Zaveri, R. A. and Peters, L. K.: A new lumped structure photochemical mechanism for large-scale
668 applications, Journal of Geophysical Research: Atmospheres, 104, 30387-30415,
669 10.1029/1999jd900876, 1999.
670 Zeng, X. and Wang, T.:RegCM-Chem-YIBS-vN2O. Zenodo. https://doi.org/10.5281/zenodo.15043206 ,
671 2025
672 Zhang, G. J., Kiehl, J. T., and Rasch, P. J.: Response of Climate Simulation to a New Convective
673 Parameterization in the National Center for Atmospheric Research Community Climate Model
674 (CCM3)*, Journal of Climate, 11, 2097-2115, 10.1175/1520-
675 0442(1998)011<2097:Rocsta>2.0.Co;2, 1998.
676 Zhang, Q., Wang, T., Wu, H., Qu, Y., Xie, M., Li, S., Zhuang, B., Li, M., and Kilifarska, N. A.: Radiative
677 and Chemical Effects of Non-Homogeneous Methane on Terrestrial Carbon Fluxes in Asia, Journal
678 of Geophysical Research: Atmospheres, 129, 10.1029/2023jd040204, 2024.
679 Zhang, Y., Wang, W., and Yao, H.: Urea-based nitrogen fertilization in agriculture: a key source of N_2O
680 emissions and recent development in mitigating strategies, Archives of Agronomy and Soil Science,
681 69, 663-678, 10.1080/03650340.2022.2025588, 2022.
682 Zhou, F., Cui, X., Shang, Z., and Wang, Q.: Spatiotemporal pattern of cropland nitrous oxide emissions:
683 Driving factors and global assessment, Journal of Agro-Environment Science, 39, 680-690,
684 10.11654/jaes.2020-0113, 2020.
685 Zhou, F., Shang, Z., Ciais, P., Tao, S., Piao, S., Raymond, P., He, C., Li, B., Wang, R., Wang, X., Peng,
686 S., Zeng, Z., Chen, H., Ying, N., Hou, X., and Xu, P.: A new high-resolution N_2O emission inventory
687 for China in 2008, Environ Sci Technol, 48, 8538-8547, 10.1021/es5018027, 2014.